

## Article

# Penidihydrocitrinins A–C: New Polyketides from the Deep-Sea-Derived *Penicillium citrinum* W17 and Their Anti-Inflammatory and Anti-Osteoporotic Bioactivities

Yong Zhang <sup>1,†</sup> , Chun-Lan Xie <sup>1,2,†</sup> , Yuan Wang <sup>1</sup>, Xi-Wen He <sup>1</sup>, Ming-Min Xie <sup>1</sup>, You Li <sup>1</sup>, Kai Zhang <sup>1</sup>, Zheng-Biao Zou <sup>1</sup>, Long-He Yang <sup>1,\*</sup>, Ren Xu <sup>2,\*</sup>  and Xian-Wen Yang <sup>1,\*</sup> 

- <sup>1</sup> Key Laboratory of Marine Genetic Resources, Technical Innovation Center for Utilization of Marine Biological Resources, Third Institute of Oceanography, Ministry of Natural Resources, 184 Daxue Road, Xiamen 361005, China; zhangyong@tio.org.cn (Y.Z.); xiechunlanxx@163.com (C.-L.X.); wy2012016284@163.com (Y.W.); hexiwen1224@163.com (X.-W.H.); xiemingmin@tio.org.cn (M.-M.X.); m220200718@st.shou.edu.cn (Y.L.); z18252730063@163.com (K.Z.); zhengbiaozou@njjust.edu.cn (Z.-B.Z.)
- <sup>2</sup> School of Medicine, Xiamen University, South Xiang'an Road, Xiamen 361005, China
- \* Correspondence: longheyang@tio.org.cn (L.-H.Y.); xuren526@xmu.edu.cn (R.X.); yangxianwen@tio.org.cn (X.-W.Y.); Tel.: +86-592-219-5319 (L.-H.Y. & X.-W.Y.); +86-592-288-0577 (R.X.)
- † These authors contributed equally to this work.

**Abstract:** Three new polyketides (penidihydrocitrinins A–C, 1–3) and fourteen known compounds (4–17) were isolated from the deep-sea-derived *Penicillium citrinum* W17. Their structures were elucidated by comprehensive analyses of 1D and 2D NMR, HRESIMS, and ECD calculations. Compounds 1–17 were evaluated for their anti-inflammatory and anti-osteoporotic bioactivities. All isolates exhibited significant inhibitory effects on LPS-stimulated nitric oxide production in murine brain microglial BV-2 cells in a dose-response manner. Notably, compound 14 displayed the strongest effect with the IC<sub>50</sub> value of 4.7 μM. Additionally, compounds 6, 7, and 8 significantly enhanced osteoblast mineralization, which was comparable to that of the positive control, purmorphamine. Furthermore, these three compounds also suppressed osteoclastogenesis in a dose-dependent manner under the concentrations of 2.5 μM, 5.0 μM, and 10 μM.

**Keywords:** deep-sea; fungus; *Penicillium citrinum*; polyketides; anti-osteoporosis; anti-inflammation



**Citation:** Zhang, Y.; Xie, C.-L.; Wang, Y.; He, X.-W.; Xie, M.-M.; Li, Y.; Zhang, K.; Zou, Z.-B.; Yang, L.-H.; Xu, R.; et al. Penidihydrocitrinins A–C: New Polyketides from the Deep-Sea-Derived *Penicillium citrinum* W17 and Their Anti-Inflammatory and Anti-Osteoporotic Bioactivities. *Mar. Drugs* **2023**, *21*, 538. <https://doi.org/10.3390/md21100538>

Academic Editors: Bin-Gui Wang and Haofu Dai

Received: 23 September 2023  
Revised: 10 October 2023  
Accepted: 12 October 2023  
Published: 14 October 2023



**Copyright:** © 2023 by the authors. Licensee MDPI, Basel, Switzerland. This article is an open access article distributed under the terms and conditions of the Creative Commons Attribution (CC BY) license (<https://creativecommons.org/licenses/by/4.0/>).

## 1. Introduction

Marine microbes are an ideal source to yield diverse secondary metabolites with unprecedented structures. As a matter of fact, about half of the new marine natural products are produced by marine microorganisms [1–3], especially those living in the deep sea under extremely tough environments such as low oxygen concentration, high salt, high hydrostatic pressure, and absence of light, which require various biochemical and physiological adaptations for survival [4,5]. These adaptations are accompanied by adjustments of gene regulation, resulting in the formation of different metabolic pathways to give birth to a large number of new secondary metabolites [4,5].

Polyketides are a class of structurally diverse natural products with carbon skeletons originating from the polymerization of short-chain carboxylic acids units, including acetate, propionate, butyrate, etc. [6], which are catalyzed by polyketide synthases (PKSs) [7]. Polyketides have attracted wide attention due to their promising bioactivities [8,9]. For example, salinosporamide A showed significant proteasomal chymotrypsin-like proteolytic inhibitory activity with an IC<sub>50</sub> value of 1.3 nM [10]; microketide A exhibited remarkable antibacterial activities against *Pseudomonas aeruginosa*, *Nocardia brasiliensis*, *Kocuria rhizophila*, and *Bacillus anthracis* with an equal minimum inhibitory concentration (MIC) value (0.19 μg/mL) to that of ciprofloxacin [11]; and theissenone exhibited potent nitric oxide production inhibitory activity in murine brain microglial BV-2 cells with an IC<sub>50</sub> value

of  $5.0 \pm 1.0 \mu\text{M}$  [12]. As some of the most abundant fungi of the world, *Penicillium* species could generate a broad spectrum of unique polyketides. For instance, two new tricyclic polyketides, penijanthinones A and B, were isolated from *P. janthinellum* HK1-6 [13,14]; two new C-8 benzoyl-substituted azaphilones, pinazaphilones A and B, were obtained from *Penicillium* sp. HN29-3B1 [13,14]; chloctanspirones A and B, possessing an unprecedented bicyclo [2.2.2] octane-2-spiro cyclohexane skeleton, were discovered in *P. terrestre* [15].

As part of our continuing discovery of structurally novel and biologically interesting compounds from deep-sea-derived microorganisms [16–20], the crude extract of *Penicillium citrinum* W17 isolated from a deep-sea sediment sample (−5278 m) of the western Pacific Ocean revealed the rich chemical diversity of the secondary metabolites. Therefore, it was subjected to a systematic chemical investigation. As a result, three new polyketides (penidihydrocitrinins A–C, 1–3) and fourteen known compounds (4–17) were obtained (Figure 1). Herein, we report the details of isolation, structure elucidation, and bioactivities of these isolates.

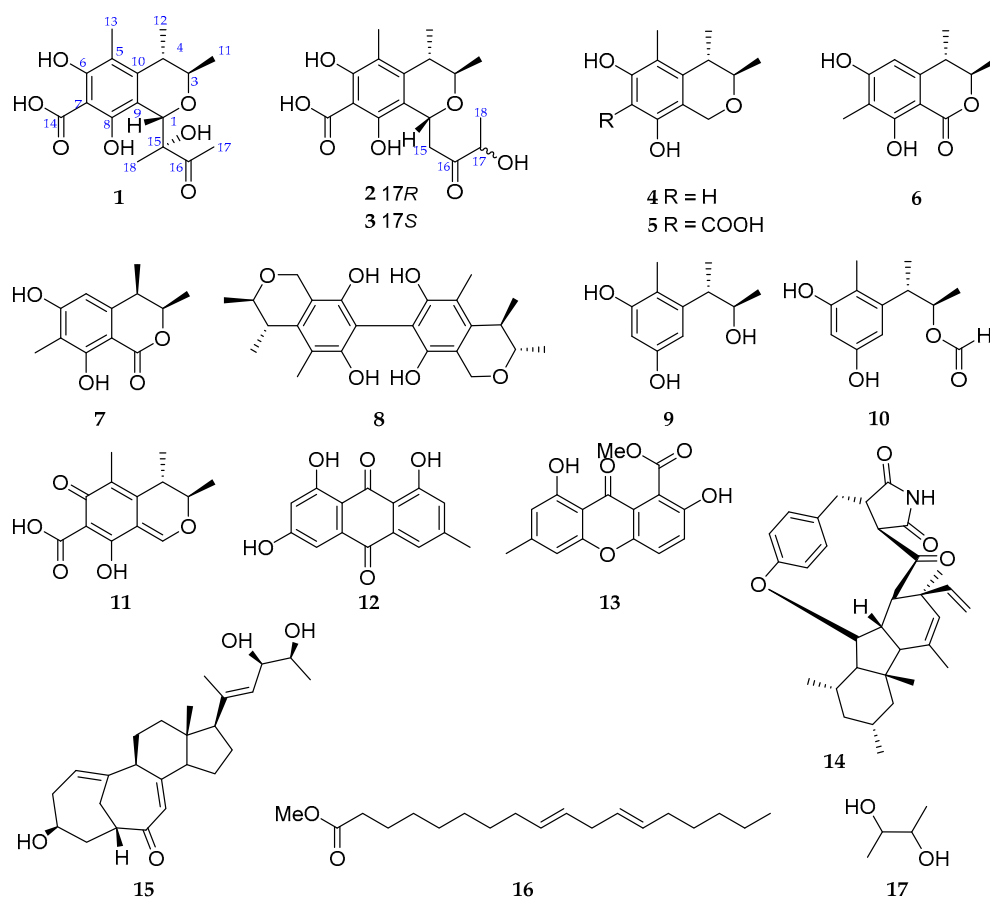


**Figure 1.** Compounds 1–17 isolated from the deep-sea-derived *Penicillium citrinum* W17.

## 2. Results and Discussion

The EtOAc-soluble extract of the deep-sea-derived *Penicillium citrinum* W17 was subjected to column chromatography (CC) on silica gel, ODS, and Sephadex LH-20, as well as preparative HPLC to afford 17 compounds (1–17).

Compound 1 was obtained as yellow amorphous powder. The molecular formula was determined as  $\text{C}_{17}\text{H}_{22}\text{O}_7$  with seven degrees of unsaturation (DoU) on the basis of HRES-IMS spectrum at  $m/z$  337.1309  $[\text{M} - \text{H}]^-$  (Figure S1 of the Supplementary Materials). The  $^1\text{H}$  NMR spectroscopic data (Table 1) showed two methyl doublets ( $\delta_{\text{H}}$  1.11 (d,  $J = 6.4$  Hz, 11-Me) and 1.28 (d,  $J = 6.9$  Hz, 12-Me)), three methyl singlets ( $\delta_{\text{H}}$  1.10 (s, 18-Me), 2.04 (s, 13-Me), and 2.30 (s, 17-Me)), and three methines ( $\delta_{\text{H}}$  2.62 (qd,  $J = 6.7$  Hz, 1.8 Hz, H-4), 3.98 (qd,  $J = 6.9$  Hz, 1.8 Hz, H-3), 5.17 (s, H-1)). The  $^{13}\text{C}$  NMR spectroscopic data exhibited

17 carbon resonance signals, including five methyls ( $\delta_C$  10.2 (q, 13-Me), 18.3 (q, 11-Me), 20.1 (q, 12-Me), 20.7 (q, 18-Me), 25.0 (q, 17-Me)), three methines ( $\delta_C$  36.9 (d, C-4), 74.0 (d, C-3), 75.4 (d, C-1)), and nine nonprotonated carbons ( $\delta_C$  83.2 (s, C-15), 102.2 (s, C-7), 110.3 (s, C-9), 114.0 (s, C-5), 143.8 (s, C-10), 156.7 (s, C-8), 160.0 (s, C-6), 178.2 (s, C-14), 211.3 (s, C-16)). The COSY correlations of 11-Me/H-3/H-4/12-Me, together with the HMBC correlations from H-4 to C-5 and C-10, from 13-Me to C-5, C-6, and C-10, from H-3 to C-10, and from H-1 to C-3, C-8, C-9, and C-10, constructed a dihydrocitricin fragment. In combination with the HMBC cross peaks of 17-Me with C-16 and of 18-Me with C-1, C-15, and C-16, the planar structure of compound **1** was established as 2-hydroxy-3-butonyldihydrocitricin (Figure 2).

**Table 1.**  $^1\text{H}$  (400 Hz) and  $^{13}\text{C}$  (100 Hz) NMR spectroscopic data of **1–3** ( $\delta$  in ppm,  $J$  in Hz within parentheses).

No.	<b>1</b> <sup>a</sup>		<b>2</b> <sup>b</sup>		<b>3</b> <sup>b</sup>	
	$\delta_C$	$\delta_H$	$\delta_C$	$\delta_H$	$\delta_C$	$\delta_H$
1	75.4 CH	5.17 s	64.8 CH	5.08 (d, 9.7)	64.8 CH	5.08 (d, 9.2)
3	74.0 CH	3.98 (qd, 6.9, 1.8)	71.7 CH	3.82 (qd, 6.6, 1.5)	71.7 CH	3.82 (qd, 6.6, 1.5)
4	36.9 CH	2.62 (qd, 6.7, 1.8)	35.1 CH	2.52 m	35.2 CH	2.51 m
5	114.0 C		109.5 C		109.6 C	
6	160.0 C		158.5 C		158.5 C	
7	102.2 C		101.8 C		101.8 C	
8	156.7 C		155.8 C		155.8 C	
9	110.3 C		110.7 C		110.9 C	
10	143.8 C		139.7 C		139.8 C	
11	18.3 CH <sub>3</sub>	1.11 (d, 6.4)	18.2 CH <sub>3</sub>	1.01 (d, 6.5)	18.3 CH <sub>3</sub>	0.99 (d, 6.5)
12	20.1 CH <sub>3</sub>	1.28 (d, 6.9)	20.1 CH <sub>3</sub>	1.17 (d, 6.8)	20.2 CH <sub>3</sub>	1.17 (d, 7.2)
13	10.2 CH <sub>3</sub>	2.04 s	9.5 CH <sub>3</sub>	1.93 s	9.6 CH <sub>3</sub>	1.92 s
14	178.2 C		175.6 C		175.7 C	
15	83.2 C		43.1 CH <sub>2</sub>	2.66 m 3.23 m	43.0 CH <sub>2</sub>	2.72 m 3.16 m
16	211.3 C		211.9 C		212.1 C	
17	25.0 CH <sub>3</sub>	2.30 s	72.2 CH	4.11 m	72.8 CH	4.02 m
18	20.7 CH <sub>3</sub>	1.10 s	19.2 CH <sub>3</sub>	1.21 (d, 7.0)	19.0 CH <sub>3</sub>	1.15 (d, 7.2)
6-OH				14.64 s		14.62 s
8-OH				15.16 s		15.13 s

<sup>a</sup> Recorded in CD<sub>3</sub>OD. <sup>b</sup> Recorded in DMSO-*d*<sub>6</sub>.

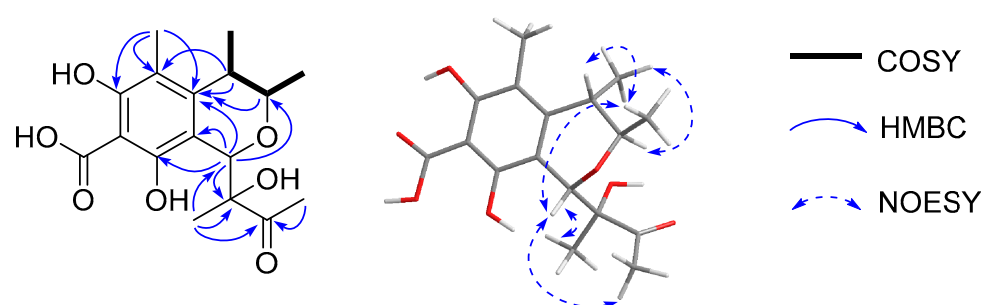


**Figure 2.** The key COSY, HMBC, and NOESY correlations of compound **1**.

The correlations of H-3/12-Me and 11-Me/H-1/H-4 were observed in the NOESY spectrum, indicating H-1, H-4, and 11-Me were on the same plane, opposite to H-3 and 12-Me (Figure 2). Although the NOESY correlations were found of H-1 to 17-Me and 18-Me, revealing the relative configuration of C-15, more solid evidence is needed to confirm the absolute configuration because of the flexible structure of the segment. Accordingly, the theoretical calculations of the electronic circular dichroism (ECD) spectrum of (1*S*,3*R*,4*S*,15*R*)-**1** and (1*S*,3*R*,4*S*,15*S*)-**1** were conducted along with their enantiomers of (1*R*,3*S*,4*R*,15*S*)-**1** and (1*R*,3*S*,4*R*,15*R*)-**1**. As shown in Figure 3, the calculated ECD spectrum of (1*S*,3*R*,4*S*,15*R*)-**1** matched well with the experimental one. On the basis of the above evidence, compound **1**

was determined as (1*S*,3*R*,4*S*,15*R*)-2-hydroxy-3-butyonyldihydrocitritin and named penidi-hydrocitritin A.

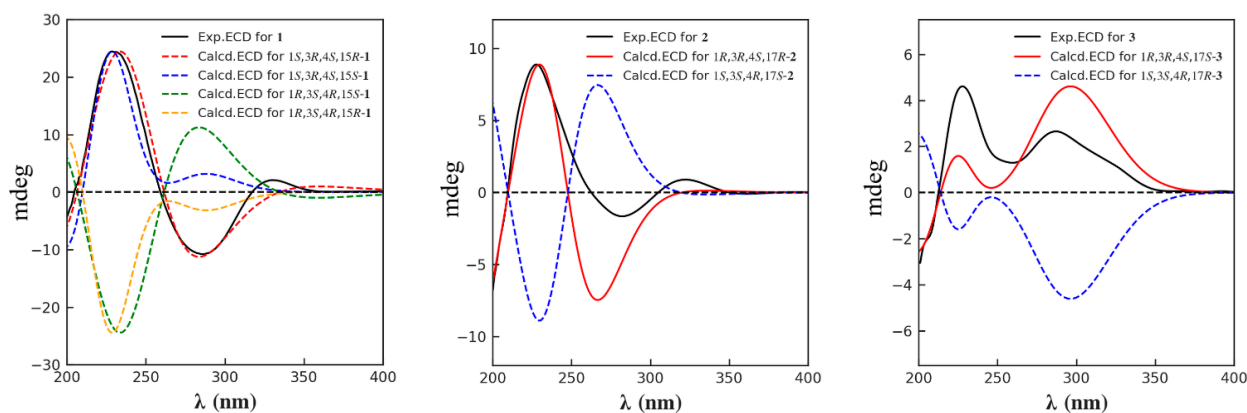


**Figure 3.** The calculated and experimental ECD spectra of compounds 1–3.

Compound **2** was obtained as a colorless oil. Its molecular formula was assigned as  $C_{17}H_{22}O_7$  on the basis of HRESIMS data at  $m/z$  337.1348  $[M - H]^-$ , suggesting seven degrees of unsaturation. Four methyls ( $\delta_H$  1.01 (d,  $J = 6.5$  Hz, 11-Me), 1.17 (d,  $J = 6.8$  Hz, 12-Me), 1.21 (d,  $J = 7.0$  Hz, 18-Me), and 1.93 (s, 13-Me)) and four methines ( $\delta_H$  2.52 (m, H-4), 3.82 (qd,  $J = 6.6$  Hz, 1.5 Hz, H-3), 4.11 (m, H-17), and 5.08 (d,  $J = 9.7$  Hz, H-1)) were recognized in the  $^1H$  NMR spectrum (Figure S9). The  $^{13}C$  NMR spectrum in association with the HSQC spectrum indicated 17 carbon signals ascribed to four methyls at  $\delta_C$  9.5 (q, 13-Me), 18.2 (q, 11-Me), 19.2 (q, 18-Me), and 20.1 (q, 12-Me); one methylene at  $\delta_C$  43.1 (t, C-15); four methines at  $\delta_C$  35.1 (d, C-4), 64.8 (d, C-1), 71.7 (d, C-3), and 72.2 (d, C-17); and eight nonprotonated carbons at  $\delta_C$  101.8 (s, C-7), 109.5 (s, C-5), 110.7 (s, C-9), 139.7 (s, C-10), 155.8 (s, C-8), 158.5 (s, C-6), 175.6 (s, C-14), and 211.9 (s, C-16). The spin systems of 11-Me/H-3/H-4/12-Me, H-17/18-Me, and H-1/H-15 were observed in the COSY spectrum, constructing three segments (Figure 4). In the HMBC spectrum, correlations were found of 13-Me to C-5/C-6/C-10, 6-OH to C-5/C-6/C-7, 8-OH to C-7/C-8/C-9, H-4 to C-3/C-5/C-10/C-12, H-1 to C-9/C-10/C-15/C-16, H-3 to C-1, and 18-Me to C-16/C-17. Taking the COSY and HMBC correlations together, the planar structure of compound **2** was then constructed as 3-hydroxy-2-butyonyldihydrocitritin, an isomer of **1**. The relative configuration of **1** was regarded as the same as that of **2** on the basis of the key NOESY correlations of H-1/11-Me, H-3/12-Me, and H-4/11-Me (Figure 4). By the biosynthetic consideration, the absolute configuration of C-1, C-3, and C-4 in **2** and **1** should be the same. However, the stereochemistry of C-17 could not be determined. Therefore, the theoretical calculation of the ECD spectrum was performed. As a result, the experimental ECD spectrum matched well with that of (1*R*,3*R*,4*S*,17*R*)-**2** (Figure 4). Consequently, the structure of **2** was assigned as (1*R*,3*R*,4*S*,17*R*)-3-hydroxy-2-butyonyldihydrocitritin and named penidi-hydrocitritin B.

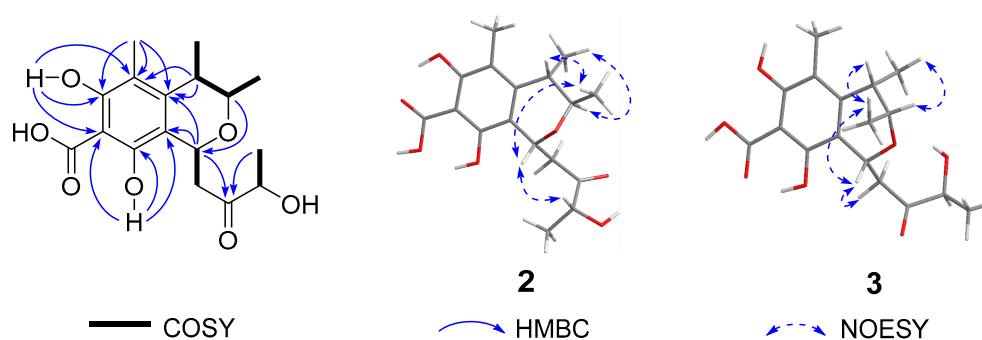
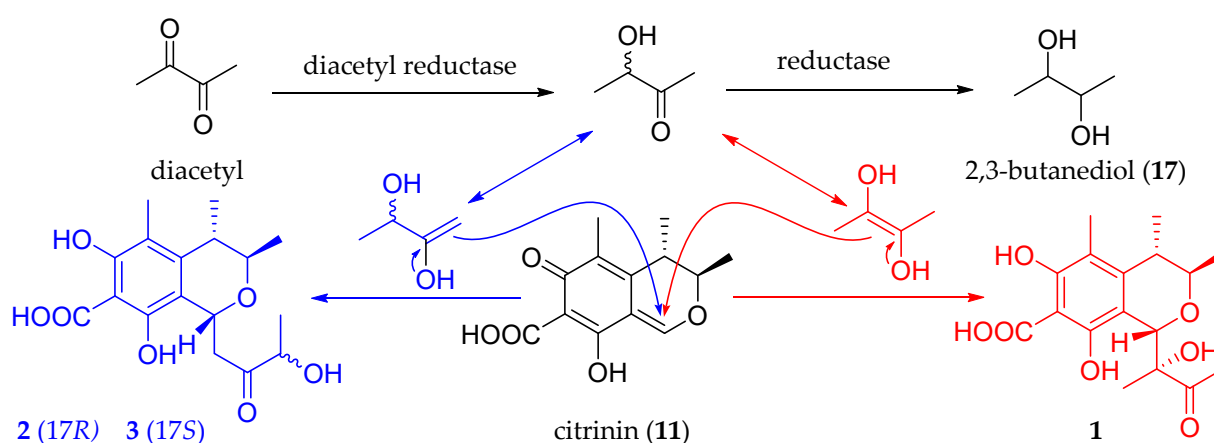


**Figure 4.** The key COSY, HMBC, and NOESY correlations of compounds **2** and **3**.

Compound **3** was isolated as a colorless oil. The molecular formula of  $C_{17}H_{22}O_7$  was established based on its HRESIMS spectrum at  $m/z$  337.1327  $[M - H]^-$  (calcd for  $C_{17}H_{21}O_7$ , 337.1287). Its  $^1H$  and  $^{13}C$  NMR spectroscopic data were very similar to those of **2**, except for the upshift of H-17 from  $\delta_H$  4.11 to  $\delta_H$  4.02 and H<sub>3</sub>-18 from  $\delta_H$  1.21 to 1.15 and the downshift of C-17 from  $\delta_C$  72.2 to 72.8. This implied that compound **3** could be an epimer of **2** with *S*-configuration at the C-17 position. The assumption was evidenced by the positive Cotton effect (CE) at  $\lambda_{max}$  287 nm ( $\Delta\epsilon$  +0.54) in **3**, whereas a negative CE ( $\Delta\epsilon$  -0.34 at  $\lambda_{max}$  282 nm) in **2**. Final confirmation was obtained by comparison of the calculated and experimental ECD spectra of **3**, showing the calculated ECD spectrum of (1*R*,3*R*,4*S*,17*S*)-**3** was in good accordance with that of the experimental curve (Figure 4). Accordingly, compound **3** was defined as (1*R*,3*R*,4*S*,17*S*)-3-hydroxy-2-butyonyldihydrocitrinin, and named penidihydrocitrinin C.

Compounds **1–3** were three novel polyketide adducts of citrinin and diacetyl. They might be biosynthesized by citrinin (**11**) and diacetyl, a widely found secondary metabolite in microorganisms [21] (Scheme 1). Noteworthy, the reduced derivative of diacetyl, 2,3-butanediol (**17**), was also co-isolated from the same extract of the strain.



**Scheme 1.** The proposed biosynthetic pathway of penidihydrocitrinins A–C (**1–3**).

By comparison of the NMR and MS data with those published in the literature, 14 known compounds were identified as decarboxydihydrocitrinin (**4**) [22], dihydrocitrinin (**5**) [23], (3*R*\*,4*S*\*)-6,8-dihydroxy-3,4,7-trimethylisocoumarin (**6**) [24], sclerotinin C (**7**) [25], asperbiphenyl (**8**) [26], phenol A (**9**) [24], citrinin H2 (**10**) [27], citrinin (**11**) [28], emodin (**12**) [29], pinselin (**13**) [30], GKK1032 B (**14**) [31], neocyclocitrinol C (**15**) [32], (*Z,Z*)-9,12-ocadecadienoic acid methyl ester (**16**) [33], and 2,3-butanediol (**17**) [34].

Microglial activation plays a pivotal role in the pathogenesis of neurodegenerative diseases, orchestrating a complex interplay between inflammation and neuronal health [35]. While microglial cells function as the guardians of the central nervous system, their dysregulated activation can lead to chronic neuroinflammation and exacerbation of neuronal damage, contributing to the progression of disorders such as multiple sclerosis and Alzheimer's and Parkinson's diseases [36]. These diseases pose significant challenges to public health, which necessitate innovative therapeutic approaches. Thus, discovering new small molecules that can inhibit the dysregulated activation of microglial cells is essential for the targeted modulation of the immune response in the central nervous system, which can reduce inflammation and protect neurons from harm [37]. A growing amount of evidence demonstrates that secondary metabolites derived from marine resources are potential therapeutic strategies for microglial-mediated neuroinflammation.

Therefore, all isolates were tested for nitrite secretion in lipopolysaccharide (LPS)-induced BV-2 microglial cells. As a result, they all demonstrated a dose-dependent suppression of nitrite secretion induced by LPS, displaying inhibitory actions at concentrations of 3.0  $\mu$ M, 10  $\mu$ M, and 20  $\mu$ M (Figure 5). Moreover, none exhibited cytotoxicity effects

against BV-2 cells at 20  $\mu\text{M}$  under the microscope. We further compared the inhibition of these compounds on nitrite production at a concentration of 10  $\mu\text{M}$  (Figure 6), and the results showed that the inhibitory rates of compounds 1–7 on nitrite production were 31.1–53.5% which indicates that substitution of the C-1 position on isochroman weakened the anti-inflammatory activity of the compounds, suggesting that this substitution is related to anti-inflammatory activity. Compound 8 only inhibited nitrite production by 26.4% in LPS-stimulated BV-2 cells, demonstrating that the dimeric structure further weakened the anti-inflammatory effect. Meanwhile, the anti-inflammatory activity of compound 12, emodin, was consistent with a previous report [38]. Notably, compound 14 (GKK1032 B) displayed the most potent nitrite inhibitory activity with an inhibitory ratio of  $73.0 \pm 1.6\%$  at 10  $\mu\text{M}$  (nitrite concentration:  $12.2 \pm 0.4 \mu\text{M}$ ), compared to the LPS-treated group (nitrite concentration:  $30.9 \pm 0.4 \mu\text{M}$ ) (Figures 5 and 6). Furthermore, this compound displayed an  $\text{IC}_{50}$  value of 4.7  $\mu\text{M}$ . Although GKK1032 analogues were reported to exhibit antibacterial activities [39], it is the first time that they had anti-neuroinflammatory activity. These findings demonstrate the effects of marine-derived compounds in modulating microglial activation, suggesting their potential as therapeutic candidates for neuroinflammatory conditions and neurodegenerative diseases.

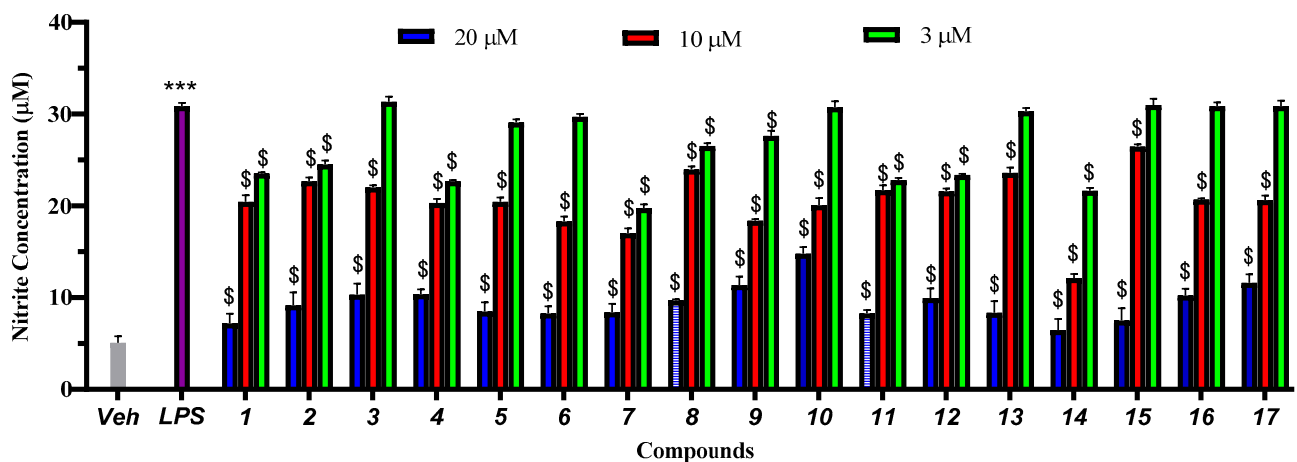


**Figure 5.** Effects of compounds 1–17 against nitrite production in LPS-induced BV-2 cells. \*\*\*  $p < 0.0001$  vs. Veh; \$  $p < 0.0001$  vs. LPS.

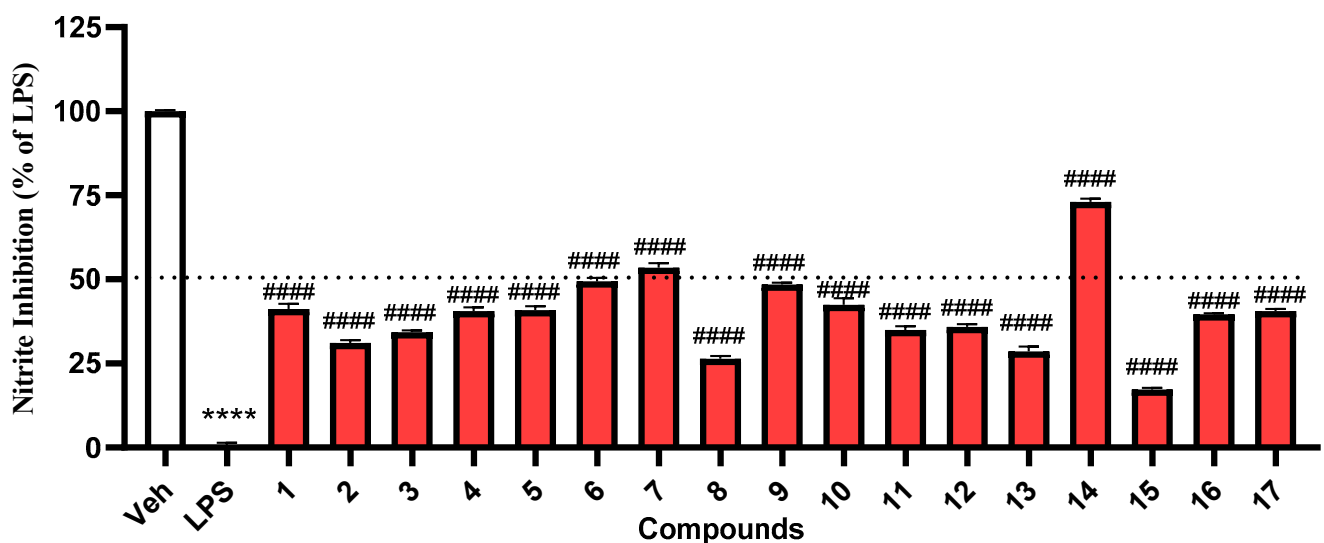


**Figure 6.** Inhibitory effects of compounds 1–17 (10  $\mu\text{M}$ ) on LPS-induced nitrite production in BV-2 cells. \*\*\*\*  $p < 0.0001$  vs. Veh; ####  $p < 0.0001$  vs. LPS.

Osteoporosis, a disease associated with aging, is characterized by excessive activation of osteoclasts or reduction of osteoblasts. Among women aged 65 or older, approximately 25% are affected by osteoporosis, with accelerated bone loss occurring after menopause. Therefore, promoting osteoblast differentiation and suppressing osteoclastogenesis are effective strategies for treating osteoporosis [40]. BMSCs are able to differentiate into osteoblasts, chondroblasts, and adipocytes [41], and bone regeneration achieved via osteogenic induction of MSCs could provide a rational therapeutic strategy for preventing age-related osteoporosis [42]. Accordingly, all 17 isolates were tested for both osteoblast and osteoclast activities. Firstly, compounds 1–17 were subjected to anti-proliferative tests on BMSCs. At the concentration of 10  $\mu\text{M}$ , none showed cytotoxicity (Figure 7).

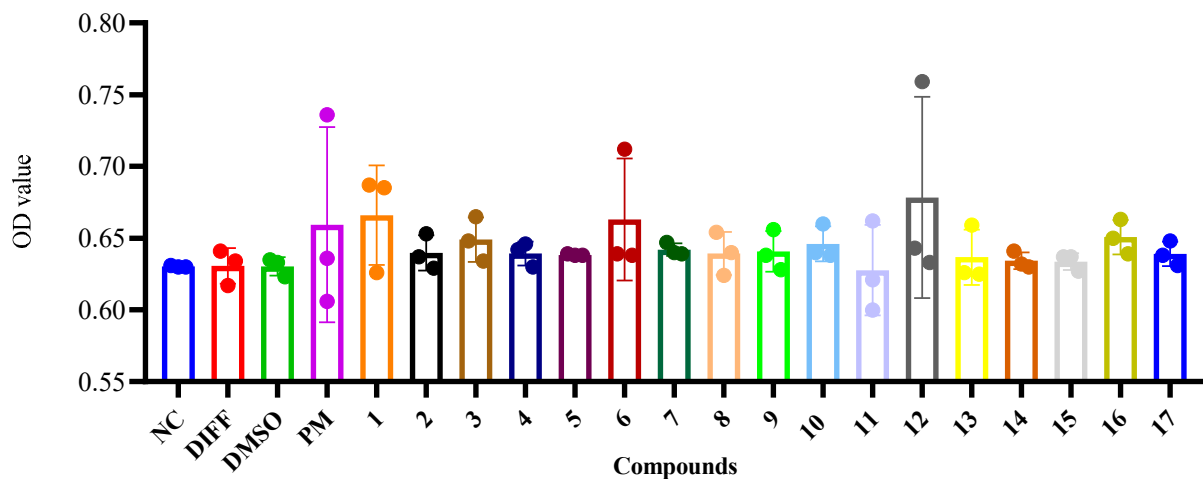


**Figure 7.** BMSC viability of compounds 1–17 was measured by the CCK-8 assay. The culture medium, osteogenesis differentiation medium (50  $\mu\text{g}/\text{mL}$  ascorbic acid and 5 mM  $\beta$ -glycerophosphate), DMSO (0.1%), and purmorphamine (1  $\mu\text{M}$ ) were regarded as the negative control (NC), differentiation (DIFF), solvent (DMSO), and positive control (PM) groups, respectively.

Intracellular calcium deposition at a later stage served as a significant evaluation indicator for osteogenic activity. Interestingly, compounds 6, 7, and 8 exerted a noticeable enhancing effect on osteoblast mineralization within BMSCs (Figure 8).

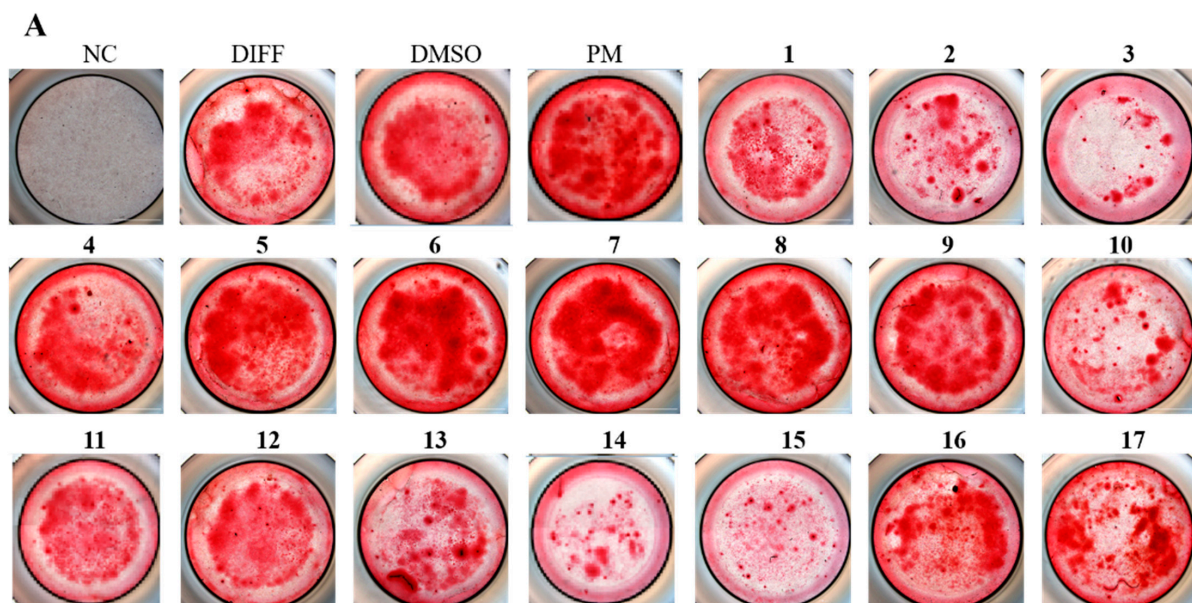


**Figure 8.** Cont.

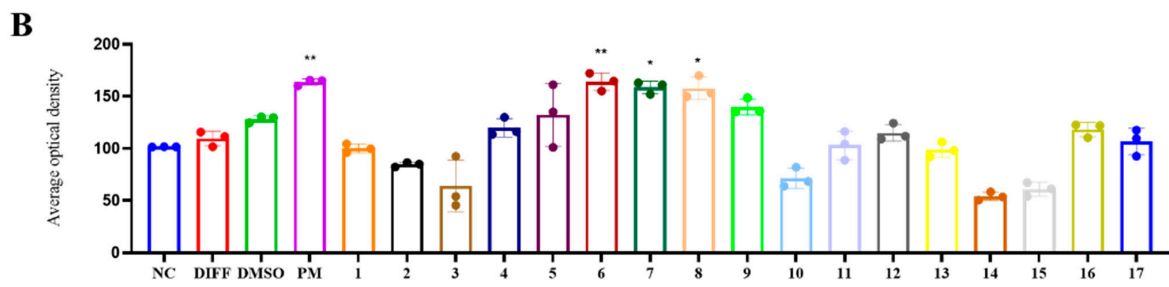


**Figure 8.** Preliminary screening results for the ability of compounds 1–17 to induce osteoblast activity among BMSCs. (A) Alizarin Red S staining. The BMSCs were cultures exposed to compounds 1–17 with osteogenic inducer. After 14 days, the cells were stained with Alizarin Red S and pictures were taken by Biotek cytation-5. The culture medium, osteogenesis differentiation medium (50 µg/mL ascorbic acid and 5 mM β-glycerophosphate), DMSO (0.1%), and purmorphamine (1 µM) were regarded as the negative control (NC), differentiation (DIFF), solvent (DMSO), and positive control (PM) groups, respectively. Scale bar = 1000 µm. (B) Quantification of Alizarin Red S staining based on average optical density. \*  $p < 0.05$ , \*\*  $p < 0.01$  vs. DMSO.

Furthermore, bioactive compounds 6, 7, and 8 also exhibited a distinct inhibitory effect on osteoclast activity, as evidenced by a significant reduction in tartrate-resistant acid phosphatase (TRAP)-positive cells (Figure 9). These findings indicate that compounds 6, 7, and 8 not only facilitated osteoblast mineralization but also exerted a substantial dose-dependent inhibitory effect on RANKL-induced osteoclasts.

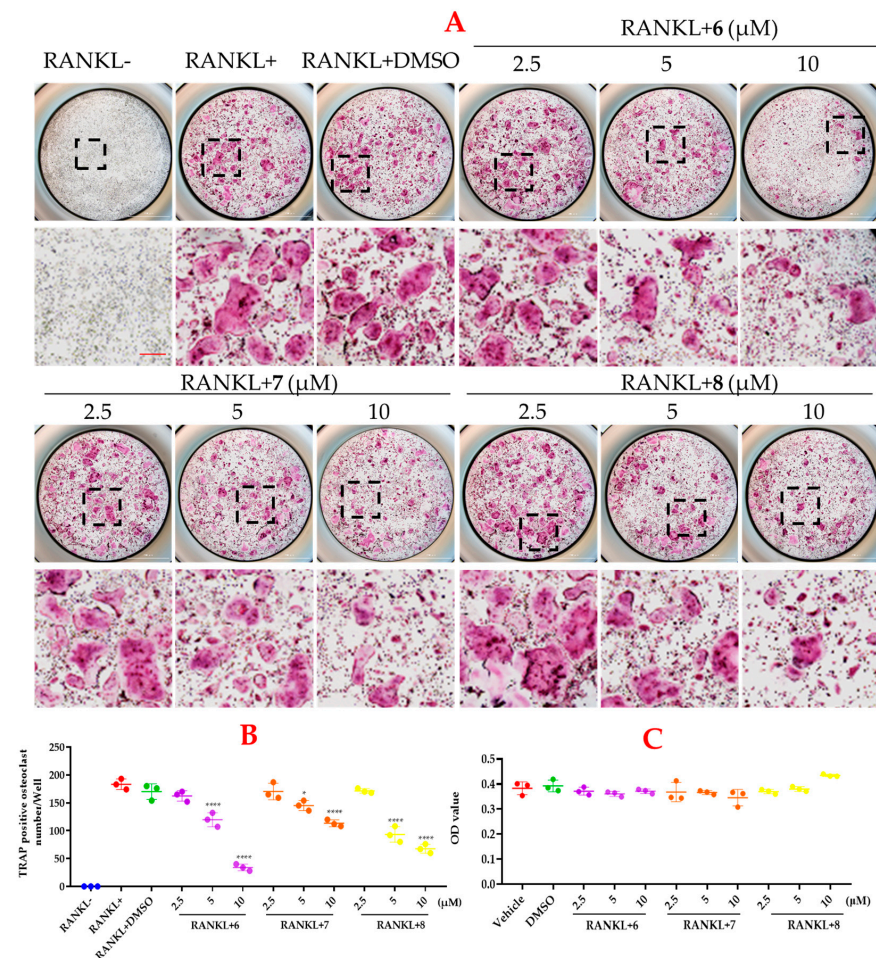


**Figure 9.** Compounds 6, 7, and 8 dose-dependently attenuated RANKL-activated osteoclastogenesis. (A) BMMs cultured with tested compounds (2.5 µM, 5.0 µM, and 10 µM) with the stimulation of

25 ng/mL RANKL (or not). After five days, these cells were fixed and stained with TRAP. (B) TRAP-positive multinucleated (three or more) cells were regarded as mature osteoclasts. Osteoclast numbers were quantified and analyzed ( $n = 3$ ). \*  $p < 0.05$ , \*\*\*\*  $p < 0.0001$  vs. the RANKL+DMSO group. (C) BMM viability was measured by the CCK-8 assay. The culture medium and the solvent (0.1% DMSO) were regarded as Vehicle and DMSO groups, respectively.

### 3. Materials and Methods

#### 3.1. General Experimental Procedures

NMR spectra of all compounds were recorded on a Bruker 400 MHz spectrometer (Bruker, Fällanden, Switzerland). Optical rotations were measured by an MCP 100 polarimeter (Anton Paar Trading Co., Ltd., Shanghai, China). The high-resolution electrospray ionization mass spectrometry (HRESIMS) results were acquired on a Xevo G2 Q-TOF mass spectrometer (Waters Corporation, Milford, MA, USA). ECD spectra were measured on a Chirascan spectrometer (Applied Photophysics, Surrey, UK). The semi-preparative high-performance liquid chromatography (semi-prep. HPLC) was performed on an Agilent instrument (1260) (Agilent Technologies, San Diego, CA, USA) with a semi-preparative chromatographic column (COSMOSIL 5 C18-MS-II, Nacalai Tesque, Japan). Column chromatography (CC) was performed on silica gel (Qingdao Marine Chemistry Co., Ltd., Qingdao, China), Sephadex LH-20 (Amersham Pharmacia Biotech AB, Uppsala, Sweden), and octadecyl silyl (ODS) (Daiso Chemical Co., Ltd., Osaka, Japan). Preparative thin-layer chromatography (Prep. TLC) was performed with silica gel precoated plates (Qingdao Marine Chemistry Co., Ltd., Qingdao, China).

#### 3.2. Fungal Identification, Fermentation, and Extraction

The fungal strain W17 was isolated from a deep-sea sediment sample of the western Pacific Ocean at the depth of 5278 m. It was identified to be *Penicillium citrinum* as the 18S rRNA gene sequence alignment (OR398934) demonstrated that it showed great similarity (99.8%) to *Penicillium citrinum* NRRL 1841 (GenBank accession number NR\_121224.1). The strain was preserved at the Key Laboratory of Marine Genetic Resources, Third Institute of Oceanography, Ministry of Natural Resources (Xiamen, China). The microbial strain was cultivated on a PDA plate medium at 25 °C for 3 days and the colony was inoculated into 250 mL Erlenmeyer flasks containing 50 mL PDB medium. Then, it was cultured in a rotary shaker (130 rpm) at 25 °C for 3 days as spore medium. After 3 days, the spore solution was inoculated in 120 Erlenmeyer flasks (1 L) with each containing 400 mL tap water, 80 g potato power, 8 g glucose, and 6 g marine salt. The fermentation was performed in a 130 rpm rotary shaker at 25 °C. After 7 days, the fermentation broth was extracted with EtOAc three times and concentrated under reduced pressure to give a crude extract (36.5 g).

#### 3.3. Isolation and Purification

The crude extract (36.5 g) was separated into seven fractions (Fr.1–Fr.7) via CC over silica gel using a gradient of CH<sub>2</sub>Cl<sub>2</sub>–MeOH (100%→75%). Fraction Fr.4 (3.6 g) was subsequently separated by CC over ODS (MeOH–H<sub>2</sub>O, 5%→100%), Sephadex LH-20 (MeOH), and semi-prep. HPLC with MeOH–H<sub>2</sub>O (40%→100%) to yield **1** (5.7 mg) and **4** (15.4 mg). Fraction Fr.7 (1.5 g) was separated by CC over Sephadex LH-20 (MeOH), silica gel (CH<sub>2</sub>Cl<sub>2</sub>–MeOH, 10:1), and semi-prep. HPLC with MeOH–H<sub>2</sub>O (30%→60%) to yield **2** (1.0 mg), **3** (1.0 mg), and **6** (45.9 mg). Compound **11** (43.0 mg) was purified from Fr.1 (5.0 g) by recrystallization in MeOH, while compounds **14** (14.0 mg) and **16** (49.0 mg) were isolated by CC over ODS (50%→100%), Sephadex LH-20 (MeOH), and prep. TLC (CH<sub>2</sub>Cl<sub>2</sub>–MeOH, 50:1). Fraction Fr.2 (2.0 g) was subjected to ODS (10%→100%) and Sephadex LH-20 (MeOH) to yield compound **12** (69.0 mg). Fraction Fr.3 was subjected to CC on ODS (10%→100%) and Sephadex LH-20 (MeOH). Final purification by semi-prep. HPLC (MeOH–H<sub>2</sub>O, 60%→90%) afforded **9** (1.6 mg) and **10** (3.7 mg). Fraction Fr.5 (4.6 g) was separated by CC over ODS (10%→100%), Sephadex LH-20 (MeOH), and semi-prep. HPLC (MeOH–H<sub>2</sub>O, 30%→60%) to give **5** (124.0 mg), **13** (7.0 mg), **15** (2.1 mg), and **17**

(190.0 mg). Compounds 7 (15.2 mg) and 8 (22.4 mg) were obtained by CC over ODS (10%→100%), Sephadex LH-20 (MeOH), and semi-prep. HPLC (MeOH–H<sub>2</sub>O, 30%→60%) from Fr.6 (2.0 g).

Penidihydrocitrinin A (1): yellow amorphous powder;  $[\alpha]_D^{25} +28.0$  (c 0.10, MeOH); UV (MeOH)  $\lambda_{max}$  (log $\epsilon$ ) 214 (3.16), 244 (2.64), 252 (2.65), 280 (1.85), 319 (2.16) nm; CD (MeOH) ( $\Delta\epsilon$ ) 229 (+5.00), 233 (+0.53), 286 (−2.20), 330 (+0.42) nm; <sup>1</sup>H and <sup>13</sup>C NMR data, see Table 1; HRESIMS  $m/z$  337.1309 [M − H]<sup>−</sup> (calcd for C<sub>17</sub>H<sub>21</sub>O<sub>7</sub> 337.1287).

Penidihydrocitrinin B (2): colorless oil;  $[\alpha]_D^{25} +25.0$  (c 0.10, MeOH); UV (MeOH)  $\lambda_{max}$  (log $\epsilon$ ) 204 (2.78), 214 (2.84), 242 (2.28), 253 (2.32), 276 (1.40), 319 (1.90) nm; CD (MeOH) ( $\Delta\epsilon$ ) 228 (+1.82), 282 (−0.34), 322 (+0.18) nm; <sup>1</sup>H and <sup>13</sup>C NMR data, see Table 1; HRESIMS  $m/z$  337.1348 [M − H]<sup>−</sup> (calcd for C<sub>17</sub>H<sub>21</sub>O<sub>7</sub> 337.1287).

Penidihydrocitrinin C (3): colorless oil;  $[\alpha]_D^{25} +40.0$  (c 0.10, MeOH); UV (MeOH)  $\lambda_{max}$  (log $\epsilon$ ) 205 (2.71), 213 (2.72), 253 (2.24), 275 (1.39), 320 (1.83) nm; CD (MeOH) ( $\Delta\epsilon$ ) 228 (+0.94), 260 (+0.26), 287 (+0.54) nm; <sup>1</sup>H and <sup>13</sup>C NMR data, see Table 1; HRESIMS  $m/z$  337.1327 [M − H]<sup>−</sup> (calcd for C<sub>17</sub>H<sub>21</sub>O<sub>7</sub>, 337.1287).

### 3.4. ECD Calculation

As reported previously [16], the conformational analysis was first conducted via random searching stochastically using the MMFF94 force field. All conformers were consecutively optimized at the PM6 and HF/6-31G(d) levels. Dominative conformers were further optimized at the B3LYP/6-31G(d) level in the gas phase. The optimized conformers possessed no imaginary frequencies and were true local minima. ECD calculations were conducted at the B3LYP/6-311G(d,p) level in MeOH with the IEFPCM model using time-dependent density functional theory (TD-DFT). The ECD spectrum was simulated by overlapping Gaussian functions for each transition.

### 3.5. BV-2 Cell Culture and Compound Treatment

BV-2 cell culture and compound treatment were carried out as previously reported [43,44]. Briefly, BV-2 microglial cells were cultured in DMEM supplemented with 10% fetal bovine serum (ThermoFisher, Shanghai, China) and antibiotics (100 units/mL of penicillin and 100 µg/mL of streptomycin) in a humidified 5% CO<sub>2</sub> incubator at 37 °C. Cells were seeded into 24-well plates at a density of 2 × 10<sup>4</sup> cells per well and allowed to adhere overnight. On the subsequent day, the cells were treated with freshly prepared culture medium containing the specified concentrations of the investigated compounds for a duration of 30 min before exposure to LPS (1 µg/mL). A control group was treated with a vehicle solution (DMSO, 0.1%).

### 3.6. Quantification of Nitrite Levels

The concentration of nitrite present in the culture medium was assessed using the Griess Reagent Kit (Thermo Fisher, Shanghai, China). Briefly, 75 µL of cell culture supernatants was mixed with an equal volume of the Griess Reagent Kit and allowed to react for 30 min at room temperature. The absorbance of the resulting diazonium compound was measured at a wavelength of 560 nm. The concentration of nitrite production was calculated based on the nitrite standard solution.

### 3.7. Cell Extraction and Culture

The bone mesenchymal stem cells (BMSCs) and bone marrow monocytes (BMMs) were flushed from the femur of C57BL/6J mice aged 3 weeks and 6-week-old C57BL/6 mice, respectively, with the methods as previously described [16]. In brief, the BMSCs were carefully removed from the animals and cultured in  $\alpha$ -MEM and induced with supplemented complete  $\alpha$ -MEM (10% v/v FBS, 1% v/v penicillin/streptomycin (P/S)). The BMSCs were induced with 2 mM  $\beta$ -glycerophosphate and 50 µg/mL ascorbate, of which half were changed twice a week. The BMMs were cultured in complete  $\alpha$ -MEM (10% v/v FBS, 1% v/v P/S, and 25 ng/mL M-CSF).

### 3.8. CCK-8 Assay

The in vitro cytotoxic bioassay was conducted using the CCK-8 method according to the previously reported protocols [16]. The BMSCs or BMMs were treated with or without compounds. After 48 h of culture, cells were treated with CCK-8 solution for 2 h before being scanned with a multimode scanner at 450 nm (Biotek, Winooski, VT, USA).

### 3.9. Osteoblast Differentiation and Mineralization

The BMSCs were digested and planted at a density of  $2 \times 10^4$  cells/well into 96-well plates and cultivated overnight. Ascorbic acid (50  $\mu\text{g}/\text{mL}$ ) and  $\beta$ -glycerophosphate (5 mM) were added into the culture medium for osteogenic assay. The culture medium was changed every other day. AR S staining was performed after 14 days of differentiation. Alizarin Red staining was used to check the calcification conditions in cultures. Cells were fixed with 10% neutral-buffered formalin for 30 min and then 2% Alizarin Red S was used to incubate cells for 2 min at room temperature. Then, pictures were taken of the cells by a Biotek cytation-5.

### 3.10. Osteoclast Differentiation

BMMs were cultured for 7 days in the presence of M-CSF (25 ng/mL) and RANKL (25 ng/mL) for differentiation into mature osteoclasts. Media were refreshed every 2 days. For tartrate-resistant acid phosphatase (TRAP) staining, cells were fixed with 4% paraformaldehyde (PFA) and stained for TRAP activity. Under a microscope (Biotek cytation-5, USA), TRAP-positive multinucleated cells with three nuclei were counted as osteoclasts.

## 4. Conclusions

In summary, from the deep-sea-derived fungus *Penicillium citrinum* W17, 17 compounds were obtained. Penidihydrocitrinins A–C (1–3) are three novel citrinin and diacetyl adducts, which greatly enrich the chemical diversity of *Penicillium* species. Compound 14 displayed potent anti-inflammatory activity. Meanwhile, 6, 7, and 8 not only significantly promoted the osteoblast mineralization but also inhibited osteoclasts, providing potent drug leads for anti-osteoporosis.

**Supplementary Materials:** The following are available online at <https://www.mdpi.com/article/10.3390/md21100538/s1>, Figures S1–S21: One-dimensional and two-dimensional NMR spectra along with HRESIMS spectra of compounds 1–3.

**Author Contributions:** X.-W.Y. designed the project; Y.Z. and Z.-B.Z. isolated and purified all compounds. C.-L.X. and R.X. conducted the anti-osteoporotic experiments; X.-W.H. and L.-H.Y. performed the anti-inflammatory bioassay. K.Z. identified the strain. Y.L. and M.-M.X. performed the fermentation. Y.Z., Y.W., and X.-W.Y. analyzed the data and wrote the paper, while critical revision of the publication was performed by all authors. All authors have read and agreed to the published version of the manuscript.

**Funding:** The work was supported by the National Key Research and Development Program of China (2022YFC2804800), the Xiamen Southern Oceanographic Center (22GYY007HJ07), and the National Natural Science Foundation of China (22177143).

**Institutional Review Board Statement:** Not applicable.

**Informed Consent Statement:** Not applicable.

**Data Availability Statement:** The data presented in this study are available in Supplementary Materials.

**Acknowledgments:** The authors wish to thank Xiao-Yong Zhang of South China Agricultural University for isolating the fungal strain and Ming-Ming Cao of Kunming Institute of Botany, Chinese Academy of Sciences for his constructive discussion on the biosynthetic pathway of the new compounds.

**Conflicts of Interest:** The authors declare no conflict of interest.

## References

1. Carroll, A.R.; Copp, B.R.; Davis, R.A.; Keyzers, R.A.; Prinsep, M.R. Marine natural products. *Nat. Prod. Rep.* **2023**, *40*, 275–325. [[CrossRef](#)] [[PubMed](#)]
2. Voser, T.M.; Campbell, M.D.; Carroll, A.R. How different are marine microbial natural products compared to their terrestrial counterparts? *Nat. Prod. Rep.* **2022**, *39*, 7–19. [[CrossRef](#)] [[PubMed](#)]
3. Carroll, A.R.; Copp, B.R.; Davis, R.A.; Keyzers, R.A.; Prinsep, M.R. Marine natural products. *Nat. Prod. Rep.* **2022**, *39*, 1122–1171. [[CrossRef](#)] [[PubMed](#)]
4. Skropeta, D.; Wei, L. Recent advances in deep-sea natural products. *Nat. Prod. Rep.* **2014**, *31*, 999–1025. [[CrossRef](#)] [[PubMed](#)]
5. Sun, C.; Mudassir, S.; Zhang, Z.; Feng, Y.; Chang, Y.; Che, Q.; Gu, Q.; Zhu, T.; Zhang, G.; Li, D. Secondary metabolites from deep-sea derived microorganisms. *Curr. Med. Chem.* **2020**, *27*, 6244–6273. [[CrossRef](#)]
6. Chooi, Y.H.; Tang, Y. Navigating the fungal polyketide chemical space: From genes to molecules. *J. Org. Chem.* **2012**, *77*, 9933–9953. [[CrossRef](#)]
7. Niu, S.; Tang, X.X.; Fan, Z.; Xia, J.M.; Xie, C.L.; Yang, X.W. Fusarisolins A-E, polyketides from the marine-derived fungus *Fusarium solani* H918. *Mar. Drugs* **2019**, *17*, 125. [[CrossRef](#)]
8. Pojer, F.; Ferrer, J.L.; Richard, S.B.; Nagegowda, D.A.; Chye, M.L.; Bach, T.J.; Noel, J.P. Structural basis for the design of potent and species-specific inhibitors of 3-hydroxy-3-methylglutaryl CoA synthases. *Proc. Natl. Acad. Sci. USA* **2006**, *103*, 11491–11496. [[CrossRef](#)]
9. De Pascale, G.; Nazi, I.; Harrison, P.H.; Wright, G.D.  $\beta$ -Lactone natural products and derivatives inactivate homoserine transacetylase, a target for antimicrobial agents. *J. Antibiot.* **2011**, *64*, 483–487. [[CrossRef](#)]
10. Feling, R.H.; Buchanan, G.O.; Mincer, T.J.; Kauffman, C.A.; Jensen, P.R.; Fenical, W. Salinosporamide A: A highly cytotoxic proteasome inhibitor from a novel microbial source, a marine bacterium of the new genus *salinospora*. *Angew. Chem. Int. Ed.* **2003**, *42*, 355–357. [[CrossRef](#)]
11. Liu, Y.F.; Zhang, Y.H.; Shao, C.L.; Cao, F.; Wang, C.Y. Mikroketides A and B, polyketides from a gorgonian-derived *Microsphaeropsis* sp. fungus. *J. Nat. Prod.* **2020**, *83*, 1300–1304. [[CrossRef](#)] [[PubMed](#)]
12. Hsieh, M.H.; Hsiao, G.; Chang, C.H.; Yang, Y.L.; Ju, Y.M.; Kuo, Y.H.; Lee, T.H. Polyketides with anti-neuroinflammatory activity from *Theissenia cinerea*. *J. Nat. Prod.* **2021**, *84*, 1898–1903. [[CrossRef](#)] [[PubMed](#)]
13. Chen, M.; Zheng, Y.Y.; Chen, Z.Q.; Shen, N.X.; Shen, L.; Zhang, F.M.; Zhou, X.J.; Wang, C.Y. NaBr-induced production of brominated azaphilones and related tricyclic polyketides by the marine-derived fungus *Penicillium janthinellum* HK1-6. *J. Nat. Prod.* **2019**, *82*, 368–374. [[CrossRef](#)] [[PubMed](#)]
14. Liu, Y.; Yang, Q.; Xia, G.; Huang, H.; Li, H.; Ma, L.; Lu, Y.; He, L.; Xia, X.; She, Z. Polyketides with  $\alpha$ -glucosidase inhibitory activity from a mangrove endophytic fungus, *Penicillium* sp. HN29-3B1. *J. Nat. Prod.* **2015**, *78*, 1816–1822. [[CrossRef](#)]
15. Li, D.; Chen, L.; Zhu, T.; Kurtán, T.; Mándi, A.; Zhao, Z.; Li, J.; Gu, Q. Chloctanspirones A and B, novel chlorinated polyketides with an unprecedented skeleton, from marine sediment derived fungus *Penicillium terrestre*. *Tetrahedron* **2011**, *67*, 7913–7918. [[CrossRef](#)]
16. He, Z.H.; Xie, C.L.; Wu, T.; Yue, Y.T.; Wang, C.F.; Xu, L.; Xie, M.M.; Zhang, Y.; Hao, Y.J.; Xu, R.; et al. Tetracyclic steroids bearing a bicyclo[4.4.1] ring system as potent antiosteoporosis agents from the deep-sea-derived fungus *Rhizopus* sp. W23. *J. Nat. Prod.* **2023**, *86*, 157–165. [[CrossRef](#)]
17. Hao, Y.J.; Zou, Z.B.; Xie, M.M.; Zhang, Y.; Xu, L.; Yu, H.Y.; Ma, H.B.; Yang, X.W. Ferroptosis inhibitory compounds from the deep-sea-derived fungus *Penicillium* sp. MCCC 3A00126. *Mar. Drugs* **2023**, *21*, 234. [[CrossRef](#)]
18. He, Z.H.; Xie, C.L.; Wu, T.; Zhang, Y.; Zou, Z.B.; Xie, M.M.; Xu, L.; Capon, R.J.; Xu, R.; Yang, X.W. Neotricitrinols A-C, unprecedented citrinin trimers with anti-osteoporosis activity from the deep-sea-derived *Penicillium citrinum* W23. *Bioorg. Chem.* **2023**, *139*, 106756. [[CrossRef](#)]
19. Xie, C.L.; Zhang, D.; Guo, K.Q.; Yan, Q.X.; Zou, Z.B.; He, Z.H.; Wu, Z.; Zhang, X.K.; Chen, H.F.; Yang, X.W. Meroterpenothiazole A, a unique meroterpenoid from the deep-sea-derived *Penicillium allii-sativi*, significantly inhibited retinoid X receptor (RXR)- $\alpha$  transcriptional effect. *Chin. Chem. Lett.* **2022**, *33*, 2057–2059. [[CrossRef](#)]
20. Niu, S.; Xie, C.L.; Xia, J.M.; Liu, Q.M.; Peng, G.; Liu, G.M.; Yang, X.W. Botryotins A-H, tetracyclic diterpenoids representing three carbon skeletons from a deep-sea-derived *Botryotinia fuckeliana*. *Org. Lett.* **2020**, *22*, 580–583. [[CrossRef](#)]
21. Wang, Y.; Sun, W.; Zheng, S.; Zhang, Y.; Bao, Y. Genetic engineering of *Bacillus* sp. and fermentation process optimizing for diacetyl production. *J. Biotechnol.* **2019**, *301*, 2–10. [[CrossRef](#)]
22. Wakana, D.; Hosoe, T.; Itabashi, T.; Okada, K.; de Campos Takaki, G.M.; Yaguchi, T.; Fukushima, K.; Kawai, K. New citrinin derivatives isolated from *Penicillium citrinum*. *J. Nat. Med.* **2006**, *60*, 279–284. [[CrossRef](#)]
23. Deruiter, J.; Jacyno, J.M.; Davis, R.A.; Cutler, H.G. Studies on aldose reductase inhibitors from fungi. I. Citrinin and related benzopyran derivatives. *J. Enzyme. Inhib.* **1992**, *6*, 201–210. [[CrossRef](#)]
24. Han, Z.; Mei, W.; Zhao, Y.; Deng, Y.; Dai, H. A new cytotoxic isocoumarin from endophytic fungus *Penicillium* SP. 091402 of the mangrove plant *Bruguiera sexangula*. *Chem. Nat. Compd.* **2010**, *45*, 805–807. [[CrossRef](#)]
25. Kuramata, M.; Fujioka, S.; Shimada, A.; Kawano, T.; Kimura, Y. Citrinolactones A, B and C, and sclerotinin C, plant growth regulators from *Penicillium citrinum*. *Biosci. Biotechnol. Biochem.* **2007**, *71*, 499–503. [[CrossRef](#)] [[PubMed](#)]
26. Wu, Z.J.; Ouyang, M.A.; Tan, Q.W. New asperxanthone and asperbiphenyl from the marine fungus *Aspergillus* sp. *Pest. Manag. Sci.* **2009**, *65*, 60–65. [[CrossRef](#)] [[PubMed](#)]

27. Hirota, M.; Menta, A.B.; Yoneyama, K.; and Kitabatake, N. A major decomposition product, citrinin H2, from citrinin on heating with moisture. *Biosci. Biotechnol. Biochem.* **2002**, *66*, 206–210. [[CrossRef](#)]
28. Chai, Y.J.; Cui, C.B.; Li, C.W.; Wu, C.J.; Tian, C.K.; Hua, W. Activation of the dormant secondary metabolite production by introducing gentamicin-resistance in a marine-derived *Penicillium purpurogenum* G59. *Mar. Drugs* **2012**, *10*, 559–582. [[CrossRef](#)]
29. Li, S.F.; Di, Y.T.; Wang, Y.H.; Tan, C.J.; Fang, X.; Zhang, Y.; Zheng, Y.T.; Li, L.; He, H.P.; Li, S.L.; et al. Anthraquinones and Lignans from *Cassia occidentalis*. *Helv. Chim. Acta* **2010**, *93*, 1795–1802. [[CrossRef](#)]
30. Kim, S.; Le, T.C.; Han, S.A.; Hillman, P.F.; Hong, A.; Hwang, S.; Du, Y.E.; Kim, H.; Oh, D.C.; Cha, S.S.; et al. Saccharobisindole, neoasterric methyl ester, and 7-chloro-4(1H)-quinolone: Three new compounds isolated from the marine bacterium *Saccharomonospora* sp. *Mar. Drugs* **2021**, *20*, 35. [[CrossRef](#)]
31. Oilawa, H. Biosynthesis of structurally unique fungal metabolite GKK1032A<sub>2</sub>: Indication of novel carbocyclic formation mechanism in polyketide biosynthesis. *J. Org. Chem.* **2003**, *68*, 3552–3557.
32. Ren, J.M.; Yang, J.K.; Zhu, H.J.; Cao, F. Bioactive steroids from the marine-derived fungus *Aspergillus flavus* JK07-1. *Chem. Nat. Compd.* **2020**, *56*, 945–947. [[CrossRef](#)]
33. Biswas, A.; Sharma, B.K.; Willett, J.L.; Erhan, S.Z.; Cheng, H.N. Room-temperature self-curing ene reactions involving soybean oil. *Green Chem.* **2008**, *10*, 290–295. [[CrossRef](#)]
34. Uemura, Y.; Sugimoto, S.; Matsunami, K.; Otsuka, H.; Takeda, Y.; Kawahata, M.; Yamaguchi, K. Microtropins A–I: 6'-O-(2''S,3''R)-2''-ethyl-2'',3''-dihydroxybutyrates of aliphatic alcohol  $\beta$ -D-glucopyranosides from the branches of *Microtropis japonica*. *Phytochemistry* **2013**, *87*, 140–147. [[CrossRef](#)]
35. Dheen, S.T.; Kaur, C.; Ling, E.A. Microglial activation and its implications in the brain diseases. *Curr. Med. Chem.* **2007**, *14*, 1189–1197. [[CrossRef](#)]
36. Rawji, K.S.; Mishra, M.K.; Michaels, N.J.; Rivest, S.; Stys, P.K.; Yong, V.W. Immunosenescence of microglia and macrophages: Impact on the ageing central nervous system. *Brain* **2016**, *139*, 653–661. [[CrossRef](#)]
37. Costa, T.; Fernandez-Villalba, E.; Izura, V.; Lucas-Ochoa, A.M.; Menezes-Filho, N.J.; Santana, R.C.; de Oliveira, M.D.; Araujo, F.M.; Estrada, C.; Silva, V.; et al. Combined 1-deoxynojirimycin and ibuprofen treatment decreases microglial activation, phagocytosis and dopaminergic degeneration in MPTP-treated mice. *J. Neuroimmune Pharmacol.* **2021**, *16*, 390–402. [[CrossRef](#)]
38. Park, S.Y.; Jin, M.L.; Ko, M.J.; Park, G.; Choi, Y.W. Anti-neuroinflammatory effect of emodin in LPS-stimulated microglia: Involvement of AMPK/Nrf2 activation. *Neurochem. Res.* **2016**, *41*, 2981–2992. [[CrossRef](#)]
39. Song, T.; Chen, M.; Ge, Z.W.; Chai, W.; Li, X.C.; Zhang, Z.; Lian, X.Y. Bioactive penicypyrrodiether A, an adduct of GKK1032 analogue and phenol A derivative, from a marine-sourced fungus *Penicillium* sp. ZZ380. *J. Org. Chem.* **2018**, *83*, 13395–13401. [[CrossRef](#)]
40. El-Desoky, A.H.H.; Tsukamoto, S. Marine natural products that inhibit osteoclastogenesis and promote osteoblast differentiation. *J. Nat. Med.* **2022**, *76*, 575–583. [[CrossRef](#)]
41. Sun, Y.; Li, Q.F.; Yan, J.; Hu, R.; Jiang, H. Isoflurane preconditioning promotes the survival and migration of bone marrow stromal cells. *Cell Physiol. Biochem.* **2015**, *36*, 1331–1345. [[CrossRef](#)] [[PubMed](#)]
42. Guan, M.; Yao, W.; Liu, R.; Lam, K.S.; Nolta, J.; Jia, J.; Panganiban, B.; Meng, L.; Zhou, P.; Shahnazari, M.; et al. Directing mesenchymal stem cells to bone to augment bone formation and increase bone mass. *Nat. Med.* **2012**, *18*, 456–462. [[CrossRef](#)] [[PubMed](#)]
43. Yang, L.H.; Ou-Yang, H.; Yan, X.; Tang, B.W.; Fang, M.J.; Wu, Z.; Chen, J.W.; Qiu, Y.K. Open-ring butenolides from a marine-derived anti-neuroinflammatory fungus *Aspergillus terreus* Y10. *Mar. Drugs* **2018**, *16*, 428. [[CrossRef](#)]
44. Niu, S.; Yang, L.; Zhang, G.; Chen, T.; Hong, B.; Pei, S.; Shao, Z. Phenolic bisabolane and cuparene sesquiterpenoids with anti-inflammatory activities from the deep-sea-derived *Aspergillus sydowii* MCCC 3A00324 fungus. *Bioorg. Chem.* **2020**, *105*, 104420. [[CrossRef](#)] [[PubMed](#)]

**Disclaimer/Publisher's Note:** The statements, opinions and data contained in all publications are solely those of the individual author(s) and contributor(s) and not of MDPI and/or the editor(s). MDPI and/or the editor(s) disclaim responsibility for any injury to people or property resulting from any ideas, methods, instructions or products referred to in the content.